





Tunable optical performance in nanosized AgInS₂-ZnS solid solution heterostructures due to the precursor's ratio modification

LIUDMILA LOGHINA,^{1,*}  MAKSYM CHYLII,¹ ANASTASIA KADERAVKOVA,¹ STANISLAV SLANG,¹  PETR SVEC,² JHONATAN RODRIGUEZ PEREIRA,¹ BOZENA FRUMAROVA,¹ AND MIROSLAV VLCEK¹

¹Center of Materials and Nanotechnologies, Faculty of Chemical Technology, University of Pardubice, nam. Cs. legii 565, Pardubice 53002, Czech Republic

²Department of General and Inorganic Chemistry, Faculty of Chemical Technology, University of Pardubice, Studentska 95, Pardubice 53210, Czech Republic

*liudmila.loghina@upce.cz

Abstract: Solid solution AgInS₂-ZnS nanostructures were prepared by reacting (Z)-1- (octadec-9-enyl)-3-phenylthiourea and 1-dodecanethiol with the corresponding metal linoleates. The combination of sulfur sources in modified ratios, which individually do not lead to significant results, resulted in the successful formation of nanorod-shaped heterostructures. The effect of sulfur source ratios on the structure, morphology, and optical properties of yellow-red emitting nanocrystals was systematically studied by X-ray diffraction (XRD), energy dispersive X-ray analysis (EDS), X-ray photoelectron spectroscopy (XPS) and scanning transmission electron microscopy (STEM) analyzes. Nanocomposite materials based on polyvinyl toluene *co*-divinylbenzene (PVT-DVB) were investigated for each of the resulting nanostructures. It was demonstrated that even traces of nanomaterial (~ 0.1 wt. %) provide a high photoluminescence quantum yield (PL QY up to 61.5%) of prepared nanocomposites.

© 2021 Optical Society of America under the terms of the [OSA Open Access Publishing Agreement](#)

1. Introduction

In the past several years, a considerable number of studies have been performed to investigate structural and optical properties of II-IV semiconductors nanocrystals (NCs) which made possible their application in diverse fields such as bioimaging [1], photonics [2], solar cells [3], light-emitting diodes (QLEDs) [4,5], scintillators [6,7], *etc.* Despite the advantages of Cd-based NCs (such as tunable bandgap over the visible wavelength range) [8,9], their intrinsic heavy metal toxicity has switched research focus to the search for nanomaterials with less toxic composition and similar properties. Ternary NCs containing elements from I-III-VI groups, such as copper or silver (CuInS₂, AgInS₂), have attracted a great interest due to their eco-friendliness, low toxicity, appropriate band-gap energies (1.53 eV and 1.87 eV, respectively) [10,11] and their long PL lifetimes [12,13]. However, the I-III-VI NCs possess relatively low PL QY possibly due to the high surface-to-volume ratio of NCs which results in surface defects [14]. Torimoto *et al.* [15] proposed to use ZnS coating to enhance the optical properties. They prepared ZnS-AgInS₂ solid solution nanoparticles with a maximum QY of 24% by thermal decomposition of (AgIn)_xZn_{2(1-x)}[S₂CN(C₂H₅)₂]₄ complexes. After that, several studies investigated the photoluminescence (PL) behavior of AgInS₂-ZnS NCs in different environments [16–18]. Very recently Soheyli *et al.* [19] reported the aqueous-based and low-temperature synthesis of different multinary AgInS-based/ZnS compounds. They demonstrated that PL emission intensity can be significantly improved by adding a suitable ZnS shell (QY up to 35%) and PL emission wavelength can be controlled by tuning the chemical composition of AgInS-based/ZnS QDs.

Comparison of absolute PL QY values as one of the most significant optical parameters was presented by Chevallier *et al.* [20] for AgInS₂-ZnS NCs series. They succeeded to enhance PL QY through the passivation of surface defects by performing ligand exchange between oleylamine and phosphine-related molecules. For red-emitting nanocrystals absolute PL QY reached 78%. Since the structural and morphological characteristics (such as size and shape) of semiconductor NCs are important parameters determining further their chemical and optical properties, developing new approaches to the controlled synthesis of AgInS₂-ZnS solid solutions has a considerable value for their industrial applications.

Herein, we report on the novel approach to the synthesis of AgInS₂-ZnS solid solution nanorods by the effective conjunction of two sulfur sources. The combination of (Z)-1-(octadec-9-enyl)-3-phenylthiourea and 1-dodecanethiol in one-pot solvothermal synthesis in different molar ratios leads to the formation of heterostructures with a uniform shape and tunable optical properties. These well-dispersed AgInS₂-ZnS solid solution nanorods exhibit excellent PL emission (relative PL QY up to 61.5%) both in a free form and embedded in a polyvinyl toluene *co*-divinylbenzene (PVT-DVB) matrix.

2. Experiment

2.1. Materials synthesis

Zinc oxide (ZnO, 99%), indium (III) acetate (In(Ac)₃, 99.9%), silver acetate (AgAc, 99.9%), 1-octadecene (ODE, technical grade, 90%), linoleic acid (LA, technical grade 60-74%), oleylamine (OAm, technical grade, 70%), 1-dodecanethiol (DDT, 99.9%), phenyl isothiocyanate (PhNCS, 99%), methylstyrene (vinyltoluene, mixture of isomers, ≥98.0%), lauroyl peroxide (Luperox LP, ≥98%) and chloroform-d (CDCl₃, 99.8 atom % D) were purchased from Merck and used without further purification. Solvents were procured from Fisher Scientific and used for the synthesis and purification of organic precursors and nanocrystals.

Synthetic procedure for the preparation of AgInS₂-ZnS heterostructures: Zinc oxide (ZnO, 2.4 mmol), linoleic acid (LA, 9.6 mol) and 1-octadecene (ODE, 7 ml) were placed in a Schlenk flask. The reaction mixture was degassed for 20 min at room temperature, then for another 20 min at 150 °C with periodic purging with Ar. After achieving complete homogenization, the reaction mixture was allowed naturally to cool down to room temperature. Indium (III) acetate (In(Ac)₃, 4 mmol) was mixed with 16 mmol LA and 10 ml ODE. Following degassing was performed upon slow heating to 100 °C and purging with Ar for 2 hours. During this time, there was a partial replacement of the anion with the release of acetic anhydride. The resulting solution was further used in all syntheses. A freshly prepared indium precursor solution (0.3 mmol, 1.12 ml), (Z)-1-(octadec-9-enyl)-3-phenylthiourea (TU, 3.6 mmol) dissolved in a mixture of oleylamine (OAm, 3.6 mmol) and ODE (from 0.5 to 2.0 ml), and silver acetate (AgAc, 0.3 mmol) were added to the resulting zinc linoleate. The calculated amount of 1-dodecanethiol (molar ratios TU : DDT = 1 : 0.5, 1 : 1, 1 : 1.5, 1 : 2 and 1 : 2.5) was introduced in one portion as the last component. The amount of injected DDT was compensated by the corresponding amount of ODE involved in the dissolution of TU. The resulting reaction mixture was degassed again for 20 min at room temperature and then slowly heated (5 °C/min) to 170 °C in an inert atmosphere for 20 minutes. From the moment the reaction mixture reached 150 °C and to the end of heating, aliquots were taken to study the growth morphology. Each sample was washed three times with acetone to remove unreacted components. Upon completion of heating, the reaction mixture was allowed naturally to cool down to room temperature. After that, it was quantitatively poured into a similar volume of chloroform, and the aggregates were separated by centrifugation. Nanocrystals were precipitated from the solution with acetone, followed by the separation of precipitate using centrifugation (10 000 rpm/7 min). The separated NCs were redissolved in CHCl₃, followed by precipitation with acetone. This purification process was repeated twice more to completely

remove unreacted precursors and solvents. The purified nanomaterial was dried *in vacuo* for 4 hours. The yield was 180 - 210 mg.

2.2. Preparation of polymer nanocomposites with embedded AgInS_2 -ZnS nanorods

0.005 g of nanomaterial, 2.85 g of VT, 0.15 g of divinylbenzene (DVB) and 0.015 g of lauroyl peroxide were placed in a thick-walled ampoule. To obtain a homogeneous solution, tightly closed ampoules were kept in an ultrasonic bath for 20 min at room temperature. Then, the ampoules containing clear solutions were mounted in a glycerol bath at room temperature and slowly heated (2 °C/min) to 80 °C. The ampoules were kept at this temperature for 1 hour and then moved in an oven (100 °C) for 12 hours to stabilize the nanocomposites.

2.3. Characterization

IR spectra in the region 3600 - 500 cm^{-1} (resolution 2 cm^{-1}) were recorded on Vertex 70v FTIR spectrometer (Bruker, Germany) using a single-bounce diamond ATR crystal. X-ray diffraction patterns (XRD) were registered using a PANalytical EMPYREAN powder X-ray diffractometer (ALMELO, Netherlands) with Cu-K α radiation ($\lambda = 1.5418 \text{ \AA}$). Energy dispersive X-ray (EDX/EDS) spectroscopy was carried out using scanning electron microscope LYRA 3 (Tescan, Czech Republic) equipped with EDS analyser Aztec X-Max 20 (Oxford Instruments) at 20 kV acceleration voltage. Scanning transmission electron microscopy (STEM) measurements of prepared NCs were acquired on the same device using a retractable STEM detector (Tescan, Czech Republic) at 30 kV acceleration voltage. The surface chemical composition of AgInS_2 -ZnS NCs was determined by X-ray photoelectron spectroscopy (XPS, ESCA 2SR, Scienta-Omicron, Germany) using a monochromatic Al-K α source (1486.6 eV). The optical properties were detected using Fluorometer PTI QuantaMaster 400 (Horiba, Germany) to obtain PL data in the spectral range 300 - 850 nm using excitation wavelength $\lambda = 300 - 500 \text{ nm}$ and UV-3600 (Shimadzu, Japan) spectrometer to get UV-VIS absorbance spectra in the spectral range 200 - 700 nm. The PL lifetime measurements were performed using TCSPC accessories for Fluorometer PTI QuantaMaster 400 with 391 nm and 456 nm light pulse excitation and the pulse duration < 1.3 ns produced by NanoLED-390 and NanoLED-450 respectively (Horiba Scientific)

3. Results and discussions

3.1. Synthesis of nanosized AgInS_2 -ZnS solid solution heterostructures

The previously presented (Z)-1-(octadec-9-enyl)-3-phenylthiourea [21] as an effective and accessible source of sulfur was used for the first time to obtain nanosized AgInS_2 -ZnS heterostructures. The mechanism of interaction of *N,N'*-disubstituted thiourea with metal carboxylates and the subsequent formation of sulfides was presented earlier [22]. Briefly, in the solvothermal synthesis carried out in a non-coordinating solvent, a bidentate complex of *N,N'*-disubstituted thiourea with metal carboxylates was formed, with its succeeding decomposition into the corresponding sulfides. Further growth of nanocrystals proceeds according to the standard scheme. The second source of sulfur, 1-dodecanethiol, in this process also acts as a *co*-ligand participating in the formation of a protective shell of nanocrystals. We suppose that in this case, the formation of metal sulfide occurs *via* the intermediate thiolate of the corresponding metal.

The decomposition of sulfur-containing complexes of Ag, In and Zn, which leads to the formation of AgInS_2 -ZnS solid solution nanorods, was recently described [23]. In our case, the formation and growth of AgInS_2 -ZnS nanorods proceed by a similar mechanism, which was confirmed by time-dependent morphological evolution experiments. The intermediate products of the synthesis carried out with the ratio TU : DDT = 1 : 1, were collected at different reaction stages: 150 °C, 170 °C - 1 min, 5 min, 10 min and 20 min. The resulting semisolid products were purified using CHCl_3 - acetone mixture and demonstrated on STEM images (Fig. 1).

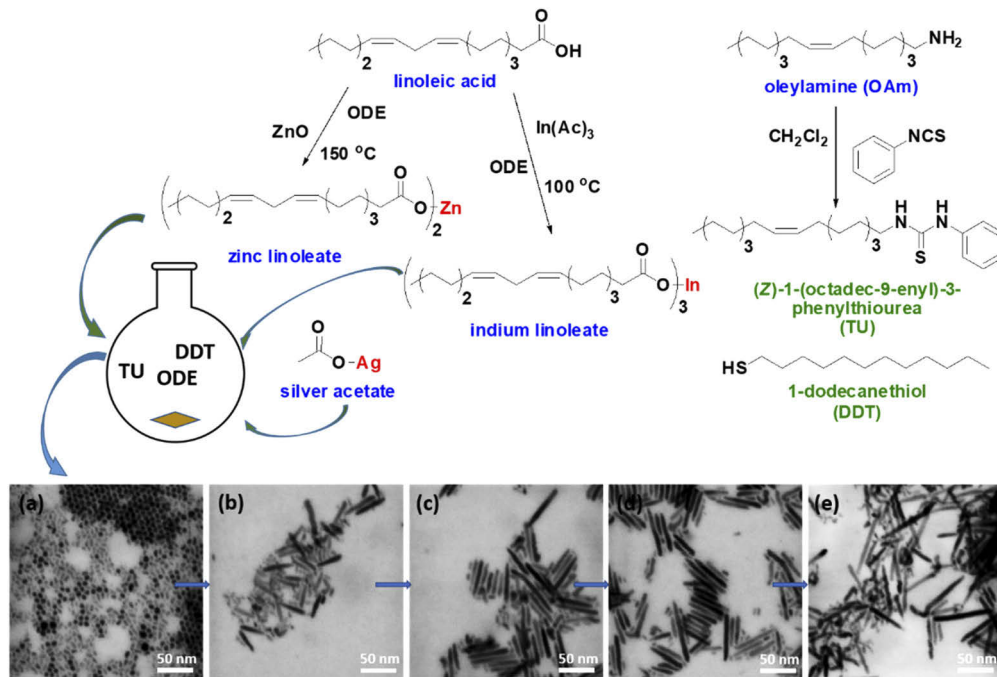


Fig. 1. Overview of $\text{AgInS}_2\text{-ZnS}$ nanorods preparation; STEM images for the probes taken from the reaction mixture at different time intervals: a) 150 °C; b) 170 °C, 1 min; c) 170 °C, 5 min; d) 170 °C, 10 min; e) 170 °C, 20 min.

As follows from Fig. 1(a)-(e), at the first step (at 150 °C) of the creation of solid solution $\text{AgInS}_2\text{-ZnS}$ heterostructures, the formation of the nanorods heads ($d_{\text{avg}} \sim 6.6$ nm) consisting of AgInS_2 -rich nanocrystals occurred. These nanocrystals served as starting seeds for further growth of solid solution nanorods. At 170 °C the elongation process of solid solution nanorods took place. Onwards, we observed the successive growth of nanorods, the length of which increases in time from 9.6 - 35.1 nm, reaching the final length $L_{\text{avg}} \sim 48.6$ nm in 20 minutes of the synthesis. It should be noted that the thickness of nanorods throughout the entire growth period remains constant and is comparable to the diameter of the nuclei ~ 6.5 nm. Throughout the synthesis, each sample contains nuclei that provide long-term heterogeneous nucleation of ZnS -rich cores depositing on the surface AgInS_2 -rich solid solution rods.

3.2. Structural analysis and morphology

Structural and morphological characterizations were carried out by X-ray powder diffraction and scanning transmission electron microscopy (STEM). Figure 2(a) represents powder X-ray diffractograms of $\text{AgInS}_2\text{-ZnS}$ solid solution nanorods prepared with different amounts of DDT. All Bragg reflections are somewhat broadened reflecting thus the small sizes of nanocrystals. Two overlapping reflections between 25° and 35° and three broad reflections between 45° and 55° were found in the corresponding diffractograms. The maxima of these peaks are in between 2 standard reflections for the bulk hexagonal ZnS (ICDD:04-007-4169) and tetragonal AgInS_2 (ICSD:605407) phases. Peaks corresponding to the tetragonal modification of AgInS_2 were detected in small quantities (see Table 1). No diffraction peaks of impurities (such as ZnO , Ag_2O , or In_2O_3) or other crystal phases were found. These results indicated that obtained $\text{AgInS}_2\text{-ZnS}$ nanorods formed a solid solution, which is in good agreement with the literature [23]. The refined lattice parameters and the calculated ratios of hexagonal and tetragonal phases are listed

in Table 1. Moreover, the diffraction pattern is maintained for all samples regardless of the significant change in the size of nanorods. As can be seen from Fig. 2(b)-(f), there is a gradual decrease in the size of nanorods with a growing content of DDT in the reaction mixture. By regulating the ratio TU : DDT, a gradual shift of the diffraction peaks to smaller angles can be observed due to an increase in the amount of AgInS₂ that forms heterostructures. It was further confirmed by the analysis of EDS data (Table 1). All four elements Ag, In, Zn, and S were detected in the samples.

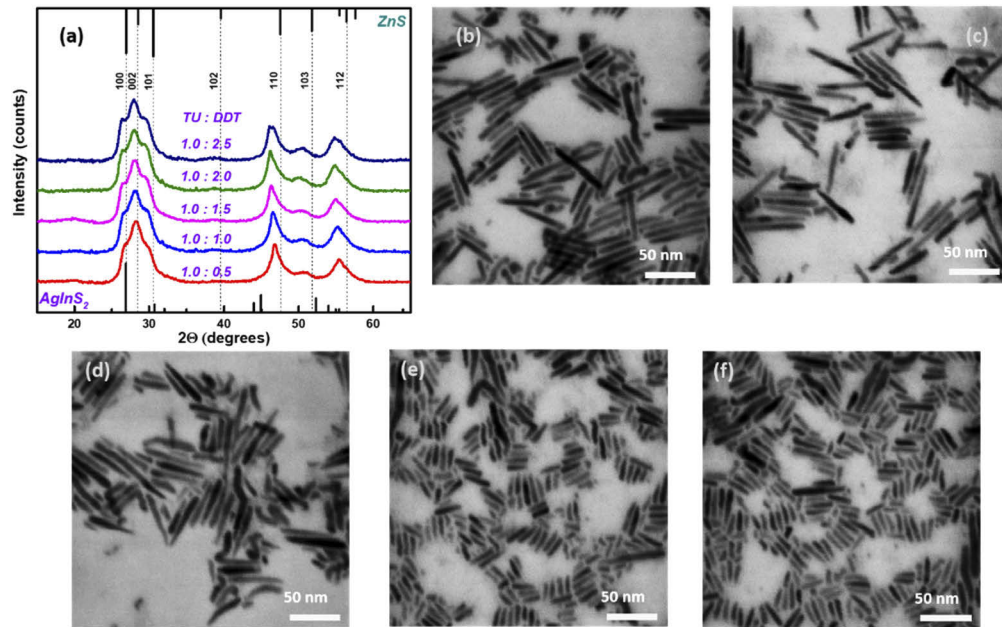


Fig. 2. XRD patterns of AgInS₂-ZnS nanorods (standard diffraction lines of hexagonal ZnS and tetragonal AgInS₂ are included for comparison) (a); STEM images of AgInS₂-ZnS nanorods synthesized with different precursor's ratio TU : DDT = 1 : 0.5 (b); 1 : 1 (c); 1 : 1.5 (d); 1 : 2 (e); 1 : 2.5 (f).

Table 1. Crystal structure results and elemental analysis measured by EDS^a

TU:DDT ratio	Phase, %	Lattice parameters			L, nm	Elemental composition			
		a, Å	b, Å	c, Å		Ag, at.%	In, at.%	Zn, at.%	S, at.%
1 : 0.5	H(96.2)	3.8968	3.8968	19.2023	55.6	3.6	5.1	43.3	48.0
	T(3.8)	6.2119	6.2119	10.6925					
1 : 1	H(96)	3.9129	3.9129	19.2477	48.6	3.2	5.5	42.1	49.2
	T(4)	6.2228	6.2228	10.8368					
1 : 1.5	H(96)	3.9339	3.9339	19.2908	44.3	4.7	6.4	39.7	49.2
	T(4)	6.2206	6.2206	10.7029					
1 : 2	H(94.6)	3.9394	3.9394	19.2442	20.7	5.6	6.7	38.3	49.4
	T(5.4)	6.2651	6.2651	10.8508					
1 : 2.5	H(94.5)	3.9069	3.9069	19.4445	17.9	4.8	6.5	38.7	50.0
	T(5.5)	6.8072	6.8072	9.8974					

^aH and T represent a hexagonal (ZnS) and tetragonal (AgInS₂) crystal structure, L – length of nanorods.

The equimolar ratios of Ag to In taken into the reaction are not the same in the final isolated products. The reason for this is that probably the different reactivity of the metal salts taken in the synthesis of AgInS₂-ZnS nanorods. The replacement of the acetate anion by thiolate will occur much faster than the replacement of the linoleic acid fragment by thiolate. The parallel formation of a bidentate complex of zinc linoleate with disubstituted thiourea will compete with the interaction of the same linoleate with thiol. Thus, there is an obvious effect of the rate difference of the precursors taken in the reaction. Also, it should be noted that with an increase in the combined sulfur precursor, there is a slight decrease in Zn at. % and a parallel increase in S at. % in AgInS₂-ZnS nanorods.

The surface chemical state of AgInS₂-ZnS nanorods was analyzed by XPS. The survey spectrum (Fig. 3(a)), reveals the presence of C, O, Zn, S, In and Ag as expected from the synthesis. The spin-orbit splitting of Ag 3d is observed at 368.0 eV (Ag 3d_{5/2}) and 374.0 eV (Ag 3d_{3/2}) corresponding to Ag¹⁺. In 3d spectrum suggests the presence of In³⁺ with In 3d_{5/2} and In 3d_{3/2} centered at 445.0 and 452.5 eV, respectively. S 2p where its spin-orbit is ascribed to S²⁻ species, since the peaks (S 2p_{3/2} and S 2p_{1/2}) are located at 162.0 and 163.2 eV. Finally, Fig. 3(a) displays Zn 2p region with two peaks that correspond to Zn 2p_{3/2} and Zn 2p_{1/2} centered at 1022.0 and 1045.0 eV, attributed to Zn²⁺ species. The binding energies of Ag 3d, In 3d, S 2p and Zn 2p in AgInS₂-ZnS nanorods are in accordance with those reported in the literature [13,24].

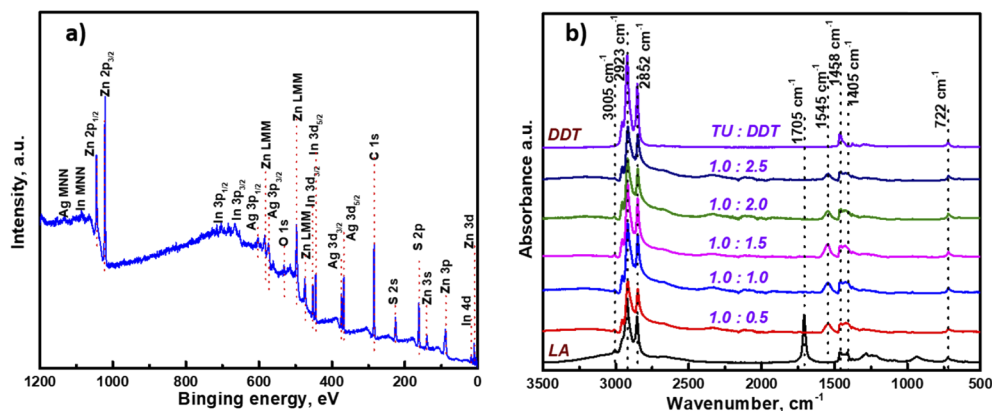


Fig. 3. XPS survey spectra of AgInS₂-ZnS nanorods (TU : DDT = 1 : 0.5) (a); FT-IR spectra of prepared nanorods in comparison with FT-IR spectra of linoleic acid (LA) and 1-dodecanethiol (DDT) (b).

The FT-IR spectra for the ligand shell of synthesized nanorods along with the spectra of LA and DDT (taken for comparison) are presented in Fig. 3(b). In all spectra of prepared samples, strong absorbance bands in the region between 3050 - 2800 cm⁻¹ were detected which are attributable to the -CH₂ groups stretching modes. For individual DDT and LA maxima of -CH₂ groups, symmetric and asymmetric stretching bands appeared at 2852 and 2923 cm⁻¹, which are correspondingly shifted to 2917 and 2848 cm⁻¹ in each spectrum of AgInS₂-ZnS nanorods. This shift to lower wavenumbers suggested that the chemisorbed alkanethiol species were more ordered on the surfaces of these nanocrystals, and probably adopted an all-trans (planar zig-zag) conformation [25,26]. In our case, the shift of -CH₂ vibration modes may indicate the presence of DDT as a capping *co*-ligand. A band at 3005 cm⁻¹ is assigned to vibrations of CH in -CH = CH-group in LA. In the fingerprints region, the absorbance band at 722 cm⁻¹ confirms the presence of (CH₂)_n alkyl chains with n > 4. Absorbance bands with maxima at 1545 cm⁻¹, 1458 cm⁻¹ and 1405 cm⁻¹ belong to the vibrations of metal carboxylate groups; the first one corresponds to asymmetric vibrations while the other two represent symmetrical vibrations. According to

Fig. 3(b), with an increase in the amount of DDT taken into the reaction, a visible drop in the intensity of the signals responsible for the vibrations of metal carboxylate groups was observed. At the same time, the intensity of the signals responsible for the vibrations of the aliphatic groups (-CH₂, -CH₃) remains practically unchanged. Consequently, a sequential replacement of the ligand occurs.

From the above mentioned, upon the interaction of metal linoleates with a significant excess of sulfur precursor, a gradual supersaturation of the nanocrystal with sulfur occurs. During the growth of already formed nuclei, metal linoleates forming a protective shell of the nanocrystal continue to interact with an excess of DDT, which is in a free form in the reaction mixture. In this case, DDT almost completely displaces metal carboxylates from the ligand shell. This phenomenon provides the passivation of the nanocrystal surface with sulfur, which in turn leads to earlier growth interruption and a decrease in the length of the nanorods.

3.3. UV-VIS and photoluminescence study

3.3.1. Nanosized AgInS₂-ZnS solid solution heterostructures

To study the influence of the TU : DDT ratios in the synthesis of AgInS₂-ZnS nanorods on their optical properties, the absorbance (ABS) and photoluminescence (PL) spectra were measured. The measurements were carried out in solutions of the same concentration (1 mg NCs / 1 ml CHCl₃). Figure 4(a) presents a comparative characteristic of the normalized spectra ABS, PL excitation (PLE) and emission of AgInS₂-ZnS nanorods prepared with the ratio TU : DDT = 1 : 0.5. There is no pronounced exciton peak in the ABS spectrum since the PL nature of such compounds is non-excitonic and comes from radiative recombination of photogenerated donor-acceptor pairs (DAP) and/or emission at surface defects [13,15,27]. The PL spectrum of the synthesized AgInS₂-ZnS nanorods has a broad emission band with maximum PL (PL_{max}) = 586 nm at PLE_{max} = 424 nm (FWHM > 100 nm). One of the advantages of this type of nanomaterials is a large Stokes shift, prepared AgInS₂-ZnS heterostructures being no exception. Estimation of the Stokes shift value was performed based on the data from excitation and emission spectra of AgInS₂-ZnS nanorods. The calculation of the band gap of direct-gap semiconductors based on the absorbance spectrum (Tauc plot) was presented earlier [21]. The experimental and calculated values of PL_{max} (λ_{em}), PLE_{max} (λ_{exc}), Stokes shift and band gap E_g are listed in Table 2.

Table 2. Optical properties of AgInS₂-ZnS nanorods and parameters of evaluation PL decay curves^a

TU:DDT ratio	Optical parameters				Fitting results of the PL decay curves						
	λ _{exc} , nm	λ _{em} , nm	Stokes shift, eV	E _g , eV	τ ₁ , ns	τ ₂ , ns	τ ₃ , ns	A ₁	A ₂	A ₃	τ _{avg} , ns
1 : 0.5	424	585	0.80	4.06	1.2	17.1	366.6	0.70	0.17	0.13	52.8
1 : 1	398	604	1.06	4.04	2.2	20.0	389.2	0.51	0.21	0.29	116.7
1 : 1.5	386	647	1.46	4.05	1.8	19.3	384.8	0.52	0.20	0.29	114.5
1 : 2	410	645	1.10	4.01	1.3	15.7	376.4	0.46	0.21	0.33	128.9
1 : 2.5	343	621	1.62	4.02	1.8	20.0	396.1	0.48	0.20	0.32	132.2

^aPeak maximum in the PLE spectra (λ_{exc}), peak maximum in the PL spectra (λ_{em}), Stokes shift and band gap (E_g); fitting results: time constants τ₁, τ₂, τ₃; amplitude components A₁, A₂ and A₃; average lifetime τ_{avg}

Figure 4(b) demonstrates a significant and nonlinear shift in PL_{max} of AgInS₂-ZnS nanorods prepared with different molar ratios of sulfur precursors. This phenomenon is related to several factors, including the size and elemental composition of nanorods. The PL_{max} of AgInS₂-ZnS nanorods synthesized with the ratio TU : DDT = 1 : 0.5 was located at 586 nm. With an increase in the DDT content within the synthesis, the PL_{max} of AgInS₂-ZnS nanorods has shifted to the red region (603 nm and 646 nm for nanorods prepared with TU : DDT = 1 : 1 and 1 : 1.5,

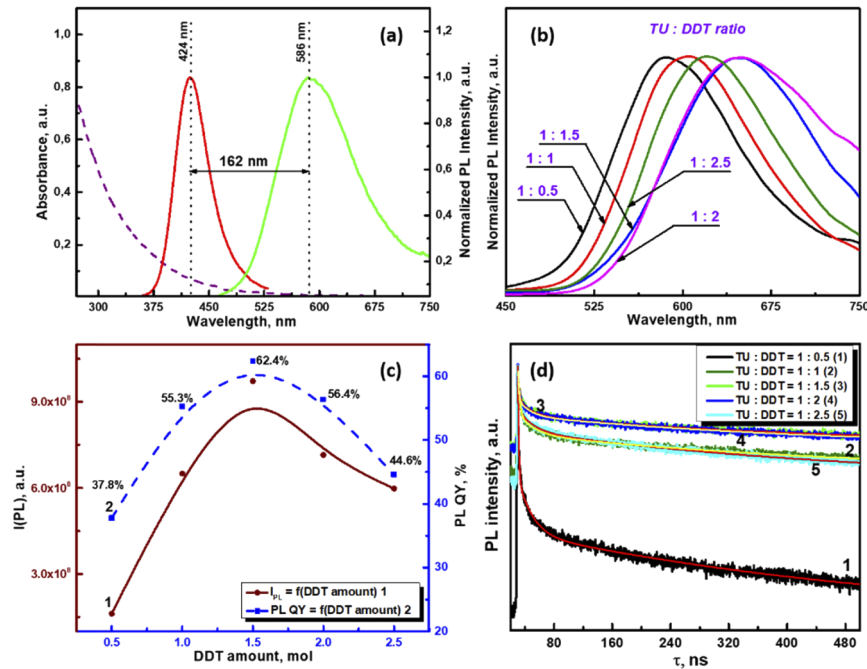


Fig. 4. Normalized ABS, PL excitation and PL emission spectra of $\text{AgInS}_2\text{-ZnS}$ solid solutions (a), normalized PL spectra of $\text{AgInS}_2\text{-ZnS}$ solid solutions prepared with different DDT content (b); PL intensity and PL QY dependences on the different DDT content (c); PL decay kinetic curves of $\text{AgInS}_2\text{-ZnS}$ solid solutions and their fitted (red and yellow) lines (d).

respectively). With a further rise of DDT amount to two equivalents ($\text{TU} : \text{DDT} = 1 : 2$), the shift of the PL_{max} to the red region has stopped, and already with the ratio $\text{TU} : \text{DDT} = 1 : 2.5$, a blue shift of the PL_{max} occurred. Possibly, this phenomenon is caused by the appearance of different number of surface defects, growing under the influence of a combination of both competing and complementary sulfur sources, as well as the influence of these defects on the recombination of photogenerated charge carriers [28]. The growing number of defects shifts the PL spectrum towards the red region ($\text{TU} : \text{DDT} = 1 : 1$ and $1 : 1.5$). With large excess of the combined sulfur sources, the nanocrystal surface is passivated with sulfur, due to which the number of defects decreases and the PL_{max} shifts to the blue region [29].

The change of the $\text{TU} : \text{DDT}$ ratios in the $\text{AgInS}_2\text{-ZnS}$ solid solution heterostructures synthesis affects not only the position of the PL maximum but also the emission intensity (Fig. 4(c)). As follows from the presented dependence, the most intense photoluminescence was possessed by $\text{AgInS}_2\text{-ZnS}$ nanorods synthesized with the ratio $\text{TU} : \text{DDT} = 1 : 1.5$.

To study the tendency to change the number of surface defects, as well as their effect on PL of synthesized $\text{AgInS}_2\text{-ZnS}$ nanorods, PL lifetime measurements were carried out. The decay kinetic curves were measured at the PL_{max} upon excitation with diode $\lambda_{\text{exc}} = 391 \text{ nm}$ (Fig. 4(d)). The PL decay kinetics curves were multi-exponential; therefore, the curves were fitted using a three-exponential function (1):

$$I(t) = y_0 + \sum_{i=1}^3 A_i e^{-\frac{t}{\tau_i}} \quad (1)$$

where τ_i and A_i are photoluminescence decay time and amplitudes. Average lifetime was calculated using the Eq. (2):

$$\tau_{avg} = \frac{\sum_{i=1}^3 A_i \tau_i}{\sum_{i=1}^3 A_i} \quad (2)$$

The fitting data are presented in Table 2. The values of chi-square goodness-of-fit are within the range of 0.95–0.97.

The presence of several components in the PL decay kinetics of AgInS₂-ZnS nanorods indicates the appearance of several defect levels with different energies and, therefore, different ways of relaxation of charge carriers in them [30,31]. The growing number of surface defects leads to an increase in the contribution of the slow time component to the PL decay kinetics and, hence, to an increase in the average lifetime. The average lifetime changes (Table 2) correlate well with the variation of PL_{max} of AgInS₂-ZnS nanorods synthesized with different TU : DDT ratios. The PL spectrum shifts to the red region (Fig. 4(b)) with a rising number of surface defects, and the average lifetime grows from 52.8 ns to 116.7 ns and 132.2 ns for AgInS₂-ZnS nanorods synthesized with TU : DDT = 1 : 1 and 1 : 1.5 ratios, respectively. With a subsequent augmentation in the DDT content in the synthesis, a decrease in the average lifetime and a blue shift of the PL_{max} of AgInS₂-ZnS nanorods were observed. This serves as evidence of the surface passivation with sulfur and the reduction of the surface defects number.

3.3.2. Polyvinyl toluene *co*-divinylbenzene based nanocomposites

Semiconductor photoluminescent nanocrystals are widely used in the production of hybrid polymer-inorganic scintillators. Such scintillators consist of a polymer matrix with photoluminescent nanoparticles embedded in it. Available and efficient scintillators with tunable characteristics can be used as components of photodetectors and high-energy radiation sensors [32,33]. In this work, well prepared AgInS₂-ZnS nanorods have an intense PL in the yellow-red spectral region and a large Stokes shift, which makes them attractive candidates for hybrid polymer-inorganic scintillators. The PL spectra of the polyvinyl toluene *co*-divinylbenzene (PVT-DVB) based nanocomposites with embedded AgInS₂-ZnS nanorods are presented in Fig. 5(a).

The PL spectra of PVT-DVB based nanocomposites were similar to the corresponding spectra of AgInS₂-ZnS nanorods (Fig. 5(a)). A slight shift of the PL_{max} of PVT-DVB based nanocomposites to the red region in comparison with the PL_{max} of dispersed in CHCl₃ AgInS₂-ZnS nanorods was observed (Table 3). The broadening of the PL spectra of PVT-DVB based nanocomposites with embedded AgInS₂-ZnS nanorods, synthesized with a large excess of DDT (Fig. 5(a), curves 4-5), was noticed. It can be caused by the interaction of sulfur on the surface of AgInS₂-ZnS nanorods with monomers during copolymerization, and, as a consequence, an increase in the number of surface defects and radiative recombination of charge carriers on them [28]. Also, the reason for the broadening of the PL signals is the superposition of both components of the nanocomposite. The PL quenching kinetic curves of PVT-DVB based nanocomposites measured at the PL_{max} are demonstrated in Fig. 5(b). As well as the PL quenching curves of AgInS₂-ZnS nanorods, the PL quenching kinetics curves of nanocomposites consist of three components. The curves were fitted similarly to the method described above. The values of chi-square goodness-of-fit are within the range of 0.95–0.98. The fitting results are presented in Table 3.

According to the fitting results, the average lifetime of PVT-DVB based nanocomposites was approximately two times shorter than the average lifetime of AgInS₂-ZnS nanorods dispersed in CHCl₃. Therefore, the incorporation of nanorods into a polymer matrix contributes to surface passivation and enhances the probability of direct and fast radiative donor-acceptor pair (DAP) recombination [32]. Figure 5(c) displays a nonlinear dependence of PL QY on the DDT amount, from which it follows that the maximum PL QY value was obtained for nanocomposites with embedded AgInS₂-ZnS nanorods synthesized with the ratio TU : DDT = 1 : 1.5. The PL QY estimation was assessed according to the standard methodology presented earlier [34] with

Table 3. Optical properties of polymer nanocomposites with embedded AgInS₂-ZnS nanorods and parameters of evaluation PL decay curves^a

TU:DDT ratio	Optical parameters				Fitting results of the PL decay curves						
	λ_{exc} , nm	λ_{em} , nm	Stokes shift, nm	PL QY, %	τ_1 , ns	τ_2 , ns	τ_3 , ns	A ₁	A ₂	A ₃	τ_{avg} , ns
1 : 0.5	377	582	1.16	41.2	1.2	13.8	308.4	0.75	0.17	0.08	28.6
1 : 1	428	615	0.87	54.1	1.6	12.1	380.2	0.68	0.20	0.13	51.4
1 : 1.5	463	690	0.89	61.5	2.0	17.5	375.0	0.65	0.18	0.17	67.3
1 : 2	399	660	1.23	49.4	1.2	14.6	359.8	0.74	0.13	0.13	49.5
1 : 2.5	464	736	0.99	52.9	1.8	11.7	368.7	0.59	0.23	0.18	68.4

^aPeak maximum in the PL spectra (λ_{exc}), peak maximum in the PL spectra (λ_{em}), Stokes shift and PL QY; fitting results: time constants τ_1 , τ_2 , τ_3 ; amplitude components A₁, A₂ and A₃; average amplitude weighted lifetime τ_{avg}

Coumarin 334 as a reference (PL QY = 0.69 in ethanol). PVT-DVB based nanocomposites have a high quantum yield (PL QY, 41.2% - 61.5%). As can be seen our PVT-DVB based nanocomposites are transparent in daylight (Fig. 5(d)) and under UV – exposure they exhibit tunable yellow-red emission (Fig. 5(e)).

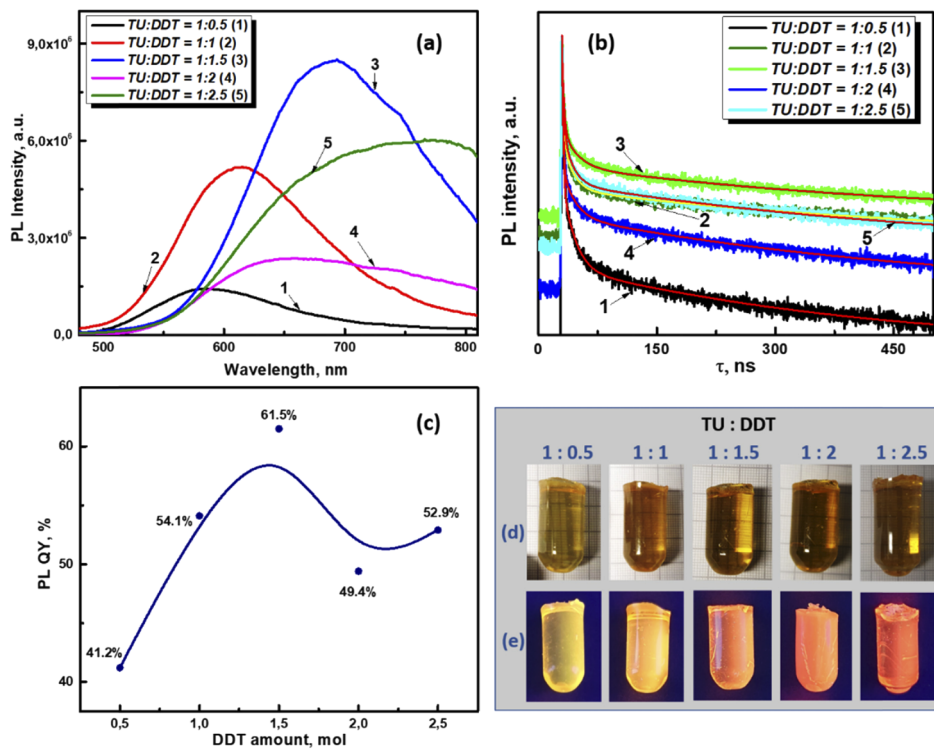


Fig. 5. PL spectra of PVT-DVB based nanocomposites with embedded AgInS₂-ZnS nanorods (a); PL decay kinetic curves of PVT-DVB based nanocomposites with embedded AgInS₂-ZnS nanorods and their fitted (red and yellow) lines (b); PL QY in dependence on the different DDT content (c); photos of the PVT-DVB nanocomposites (thickness ~ 1 cm) with embedded AgInS₂-ZnS nanorods in daylight (d) and UV-exposed (e) samples.

Conclusions

To conclude, an efficient approach to the synthesis of AgInS₂-ZnS solid solution nanorods based on the combination of two environmentally friendly sulfur sources has been demonstrated. Available (Z)-1-(octadec-9-enyl)-3-phenylthiourea obtained with a quantitative yield can serve as an excellent substitute for less reactive sources of sulfur in the synthesis of semiconductor nanomaterials. The variation of the ratios of (Z)-1-(octadec-9-enyl)-3-phenylthiourea and 1-dodecanethiol in the synthesis of nanosized AgInS₂-ZnS solid solution heterostructures led to an almost linear shift of the composition towards AgInS₂, a consistent decrease in length, and, with a large excess DDT, to growth interruption of nanorods. It has been found that with large excesses of DDT, there is a partial displacement of metal carboxylates from the protective shell of nanorods with simultaneous passivation of the surface with sulfur. Yellow-red emitting highly photoluminescent nanorods have a large Stokes shift, which makes them attractive candidates for the fabrication of hybrid polymer-inorganic scintillators. AgInS₂-ZnS solid solution nanorods were easily incorporated into the polymer matrix without loss in PL QY (up to 61.5%). Our research thus provides an efficient and convenient way for the controlled synthesis of AgInS₂-ZnS solid solution nanorods and their future industrial applications.

Funding. Ministerstvo Školství, Mládeže a Tělovýchovy (CZ.02.1.01/0.0/0.0/17_048/0007376, LM2018103).

Acknowledgments. Authors appreciate financial support from the project “High-sensitive and low-density materials based on polymeric nanocomposites” - NANOMAT (No. CZ.02.1.01/0.0/0.0/17_048/0007376) and grant LM2018103 from the Ministry of Education, Youth and Sports of the Czech Republic.

Disclosures. The authors declare no conflicts of interest.

References

1. I. L. Medintz, H. T. Uyeda, E. R. Goldman, and H. Mattoussi, “Quantum dot bioconjugates for imaging, labelling and sensing,” *Nat. Mater.* **4**(6), 435–446 (2005).
2. P. Prabhakaran, W. J. Kim, K.-S. Lee, and P. N. Prasad, “Quantum dots (QDs) for photonic applications,” *Opt. Mater. Express* **2**(5), 578 (2012).
3. I. Lokteva, N. Radychev, F. Witt, H. Borchert, J. Parisi, and J. Kolny-Olesiak, “Surface Treatment of CdSe Nanoparticles for Application in Hybrid Solar Cells: The Effect of Multiple Ligand Exchange with Pyridine,” *J. Phys. Chem. C* **114**(29), 12784–12791 (2010).
4. Q. Sun, Y. A. Wang, L. S. Li, D. Wang, T. Zhu, J. Xu, C. Yang, and Y. Li, “Bright, multicoloured light-emitting diodes based on quantum dots,” *Nat. Photonics* **1**(12), 717–722 (2007).
5. X. Jin, H. Li, S. Huang, X. Gu, H. Shen, D. Li, X. Zhang, Q. Zhang, F. Li, and Q. Li, “Bright alloy type-II quantum dots and their application to light-emitting diodes,” *J. Colloid Interface Sci.* **510**, 376–383 (2018).
6. C. Liu, Z. Li, T. J. Hajagos, D. Kishpaugh, D. Y. Chen, and Q. Pei, “Transparent Ultra-High-Loading Quantum Dot/Polymer Nanocomposite Monolith for Gamma Scintillation,” *ACS Nano* **11**(6), 6422–6430 (2017).
7. L. B. Matyushkin and N. M. Romanov, “Effect of gamma irradiation on the photoluminescence of CsPbBr₃ and CdSe/ZnS nanocrystals,” *J. Opt. Technol.* **85**(2), 119 (2018).
8. L. Loghina, A. Iakovleva, M. Chylil, P. Svec, J. Houdek, S. Slang, K. Palka, J. Michalicka, and M. Vlcek, “Synthetic development in Cd–Zn–Se quantum dots chemistry,” *Opt. Mater. (Amsterdam, Neth.)* **97**, 109385 (2019).
9. S. Slang, L. Loghina, K. Palka, and M. Vlcek, “Exposure enhanced photoluminescence of CdS_{0.9}Se_{0.1} quantum dots embedded in spin-coated Ge₂₅S₇₅ thin films,” *RSC Adv.* **7**(85), 53830–53838 (2017).
10. J. Zhang, R. Xie, and W. Yang, “A Simple Route for Highly Luminescent Quaternary Cu-Zn-In-S Nanocrystal Emitters,” *Chem. Mater.* **23**(14), 3357–3361 (2011).
11. F. Li, C. Guo, R. Pan, Y. Zhu, L. You, J. Wang, X. Jin, Q. Zhang, Y. Song, Z. Chen, and Q. Li, “Integration of green CuInS₂/ZnS quantum dots for high-efficiency light-emitting diodes and high-responsivity photodetectors,” *Opt. Mater. Express* **8**(2), 314 (2018).
12. M. Sandroni, K. D. Wegner, D. Aldakov, and P. Reiss, “Prospects of Chalcopyrite-Type Nanocrystals for Energy Applications,” *ACS Energy Lett.* **2**(5), 1076–1088 (2017).
13. Y. Yang, Y. Liu, B. Mao, B. Luo, K. Zhang, W. Wei, Z. Kang, W. Shi, and S. Yuan, “Facile Surface Engineering of Ag–In–Zn–S Quantum Dot Photocatalysts by Mixed-Ligand Passivation with Improved Charge Carrier Lifetime,” *Catal. Lett.* **149**(7), 1800–1812 (2019).
14. S. Jain, S. Bharti, G. K. Bhullar, and S. K. Tripathi, “I-III-VI core/shell QDs: Synthesis, characterizations and applications,” *J. Lumin.* **219**, 116912 (2020).
15. T. Torimoto, T. Adachi, K. Okazaki, M. Sakuraoaka, T. Shibayama, B. Ohtani, A. Kudo, and S. Kuwabata, “Facile Synthesis of ZnS–AgInS₂ Solid Solution Nanoparticles for a Color-Adjustable Luminophore,” *J. Am. Chem. Soc.* **129**(41), 12388–12389 (2007).

16. T. Uematsu, S. Taniguchi, T. Torimoto, and S. Kuwabata, "Emission quench of water-soluble ZnS–AgInS₂ solid solution nanocrystals and its application to chemosensors," *Chem. Commun.* **28**(48), 7485 (2009).
17. J.-Y. Chang, G.-Q. Wang, C.-Y. Cheng, W.-X. Lin, and J.-C. Hsu, "Strategies for photoluminescence enhancement of AgInS₂ quantum dots and their application as bioimaging probes," *J. Mater. Chem.* **22**(21), 10609 (2012).
18. T. Torimoto, S. Ogawa, T. Adachi, T. Kameyama, K. Okazaki, T. Shibayama, A. Kudo, and S. Kuwabata, "Remarkable photoluminescence enhancement of ZnS–AgInS₂ solid solution nanoparticles by post-synthesis treatment," *Chem. Commun.* **46**(12), 2082 (2010).
19. E. Soheyli, B. Ghaemi, R. Sahraei, Z. Sabzevari, S. Kharrazi, and A. Amani, "Colloidal synthesis of tunably luminescent AgInS-based/ZnS core/shell quantum dots as biocompatible nano-probe for high-contrast fluorescence bioimaging," *Mater. Sci. Eng., C* **111**, 110807 (2020).
20. T. Chevallier, G. Le Blevenec, and F. Chandezon, "Photoluminescence properties of AgInS₂–ZnS nanocrystals: the critical role of the surface," *Nanoscale* **8**(14), 7612–7620 (2016).
21. A. Iakovleva, L. Loghina, Z. Olmrova Zmrhalova, J. Mistrik, P. Svec, S. Slang, K. Palka, and M. Vlcek, "Environmentally friendly approach to the synthesis of monodisperse and bright blue emitting Cd_{0.15}Zn_{0.85}S quantum dots," *J. Alloys Compd.* **812**, 152159 (2020).
22. L. Loghina, M. Grinco, A. Iakovleva, S. Slang, K. Palka, and M. Vlcek, "Mechanistic investigation of the sulfur precursor evolution in the synthesis of highly photoluminescent Cd_{0.15}Zn_{0.85}S quantum dots," *New J. Chem.* **42**(18), 14779–14788 (2018).
23. X. Yang, Y. Tang, S. T. Tan, M. Bosman, Z. Dong, K. S. Leck, Y. Ji, H. V. Demir, and X. W. Sun, "Facile Synthesis of Luminescent AgInS₂-ZnS Solid Solution Nanorods," *Small* **9**(16), 2689–2695 (2013).
24. T. Huang, Y. Hua, J. Yao, Y. Luo, and X. Liu, "The synergetic effect of graphene and MoS₂ on AgInZnS for visible-light driven photocatalytic H₂ evolution," *Mater. Chem. Phys.* **212**, 506–512 (2018).
25. M. D. Porter, T. B. Bright, D. L. Allara, and C. E. D. Chidsey, "Spontaneously organized molecular assemblies. 4. Structural characterization of n-alkyl thiol monolayers on gold by optical ellipsometry, infrared spectroscopy, and electrochemistry," *J. Am. Chem. Soc.* **109**(12), 3559–3568 (1987).
26. S. W. Han, Y. Kim, and K. Kim, "Dodecanethiol-Derivatized Au/Ag Bimetallic Nanoparticles: TEM, UV/VIS, XPS, and FTIR Analysis," *J. Colloid Interface Sci.* **208**(1), 272–278 (1998).
27. T. Kameyama, T. Takahashi, T. Machida, Y. Kamiya, T. Yamamoto, S. Kuwabata, and T. Torimoto, "Controlling the Electronic Energy Structure of ZnS–AgInS₂ Solid Solution Nanocrystals for Photoluminescence and Photocatalytic Hydrogen Evolution," *J. Phys. Chem. C* **119**(44), 24740–24749 (2015).
28. Y. Hamanaka, K. Ozawa, and T. Kuzuya, "Enhancement of Donor–Acceptor Pair Emissions in Colloidal AgInS₂ Quantum Dots with High Concentrations of Defects," *J. Phys. Chem. C* **118**(26), 14562–14568 (2014).
29. L. Loghina, A. Kaderavkova, M. Chylii, B. Frumarova, P. Svec, S. Slang, and M. Vlcek, "The systematic study of the precursor ratio effect in the Cd–Zn–S quantum dot synthesis," *CrystEngComm* **22**(25), 4324–4337 (2020).
30. A. P. Gaikwad, D. Tyagi, C. A. Betty, and R. Sasikala, "Photocatalytic and photo electrochemical properties of cadmium zinc sulfide solid solution in the presence of Pt and RuS₂ dual co-catalysts," *Appl. Catal., A* **517**, 91–99 (2016).
31. A. J. Wojtowicz, J. Glodo, W. Drozdowski, and K. R. Przegietka, "Electron traps and scintillation mechanism in YAlO₃:Ce and LuAlO₃:Ce scintillators," *J. Lumin.* **79**(4), 275–291 (1998).
32. D. Aldakov, A. Lefrançois, and P. Reiss, "Ternary and quaternary metal chalcogenide nanocrystals: synthesis, properties and applications," *J. Mater. Chem. C* **1**(24), 3756 (2013).
33. E. Zanazzi, M. Favaro, A. Ficarelli, L. Pancheri, G. F. Dalla Betta, and A. Quaranta, "Real-Time Optical Response of Polysiloxane/Quantum Dot Nanocomposites under 2 MeV Proton Irradiation: Luminescence Enhancement of Polysiloxane Emission through Quantum Dot Sensitization," *Phys. Status Solidi A* **217**(5), 1900586 (2020).
34. A. Kaderavkova, L. Loghina, M. Chylii, S. Slang, P. Placek, B. Frumarova, and M. Vlcek, "N,N',N'-trisubstituted thiourea as a novel sulfur source for the synthesis of Mn-doped ZnS QDs," *J. Alloys Compd.* **831**, 154814 (2020).